Journal of Manufacturing Processes 119 (2024) 649–665

Contents lists available at ScienceDirect

Journal of Manufacturing Processes

journal homepage: www.elsevier.com/locate/manpro

Fan-out panel-level package warpage and reliability analyses considering the fabrication process

Chia-Wei Liang [a], Yu-Chi Sung [a], Sheng-Jye Hwang [a,*], Ming-Hsiang Shih [b], Wen-Hsiang Liao [b], Te-Hsun Lin [b], Dong-Yan Yang [b]

[a] Department of Mechanical Engineering, National Cheng Kung University, Tainan, Taiwan
[b] Testing Center, Innolux Corporation, Tainan, Taiwan

ARTICLE INFO

Keywords:
Fan-out panel-level packaging
Redistribution layer-first
Epoxy molding compound
Pressure–volume–temperature–cure equations
Residual stress
Fatigue life

ABSTRACT

With the continuous advancement of IC packaging technology, 3D and 2.5D packaging systems have emerged as the prevailing trends. The advantages of large area and high I/O density have made fan-out panel-level packaging (FOPLP) been considered as one of the best package types for 3D and 2.5D packaging applications. The discussions about FOPLP have been popular recently. Warpage and reliability of FOPLP are the main concerns of packaging engineers. However, it was found that warpage and reliability of FOPLP are strongly related to the fabrication process but not many research works have been published. Thus, reliability analysis procedure considering the residual stress of fabrication process was proposed in this paper to observe warpage and stress distribution during fabrication process. Then, this research procedure facilitates subsequent fatigue life calculations and predicts reliability of the package.

First, the thermal stresses and warpage of the redistribution layer-first (RDL-first) process were conducted for an entire panel. Next, warpage and thermal stress analyses were conducted for a strip encapsulated with an epoxy molding compound (EMC) during compression molding. Then, a reliability analysis was conducted with an IC unit and incorporated the consideration of the residual stress induced during the fabrication processes.

The compression molding analysis utilized the pressure–volume–temperature–cure (P–V–T–C) model to account for both the volume shrinkage caused by a thermal mismatch and the chemical shrinkage. Furthermore, dual shift factor model was used to model the viscoelastic behavior of EMC in this study during PMC analysis effectively.

An observation of the stress distribution for an IC unit revealed that the maximum stress position was at the solder ball near the periphery, with a stress value of 147.309 MPa. The fatigue life calculated using the modified Coffin–Manson fatigue model was 417 cycles.

1. Introduction

With the continuous advancement of IC packaging technology, 3D and 2.5D packaging systems have emerged as the prevailing trends in the recent years. The design of electronic structures is progressively moving toward thinner and shorter dimensions. Consequently, packaging technologies that offer reduced package size and high-density integration hold significant advantages in this context.

FOPLP can be categorized into two methods: the “molding-first” and the “RDL-first” [1,2] approaches, which differ primarily in terms of their molding sequences. This research focused on the RDL-first process in FOPLP. In the RDL-first method, the RDL layer and chip are first stacked on the carrier board, and subsequently, the chip is over-molded, and the carrier is removed. RDL-first offers the advantage of constructing the RDL on a flat carrier initially, resulting in improved warpage control and a high design yield. This approach is commonly used for chips with a high I/O density as it helps prevent potential chip loss and streamline the manufacturing process; Fig. 1 illustrates the relevant schematic representation [3].

Hong and Hwang [4] used the *P–V–T–C* relationship to accurately predict the warpage and residual stress of a double-layer plate structure. The equal importance of volume shrinkage results from the curing reaction of epoxy molding compound (EMC) and thermal expansion; thus, when conducting the simulation analysis, it was crucial to consider this

* Corresponding author.
E-mail address: jimppl@mail.ncku.edu.tw (S.-J. Hwang).

https://doi.org/10.1016/j.jmapro.2024.03.070
Received 12 December 2023; Received in revised form 17 March 2024; Accepted 20 March 2024
Available online 8 April 2024
1526-6125/© 2024 The Society of Manufacturing Engineers. Published by Elsevier Ltd. All rights reserved.

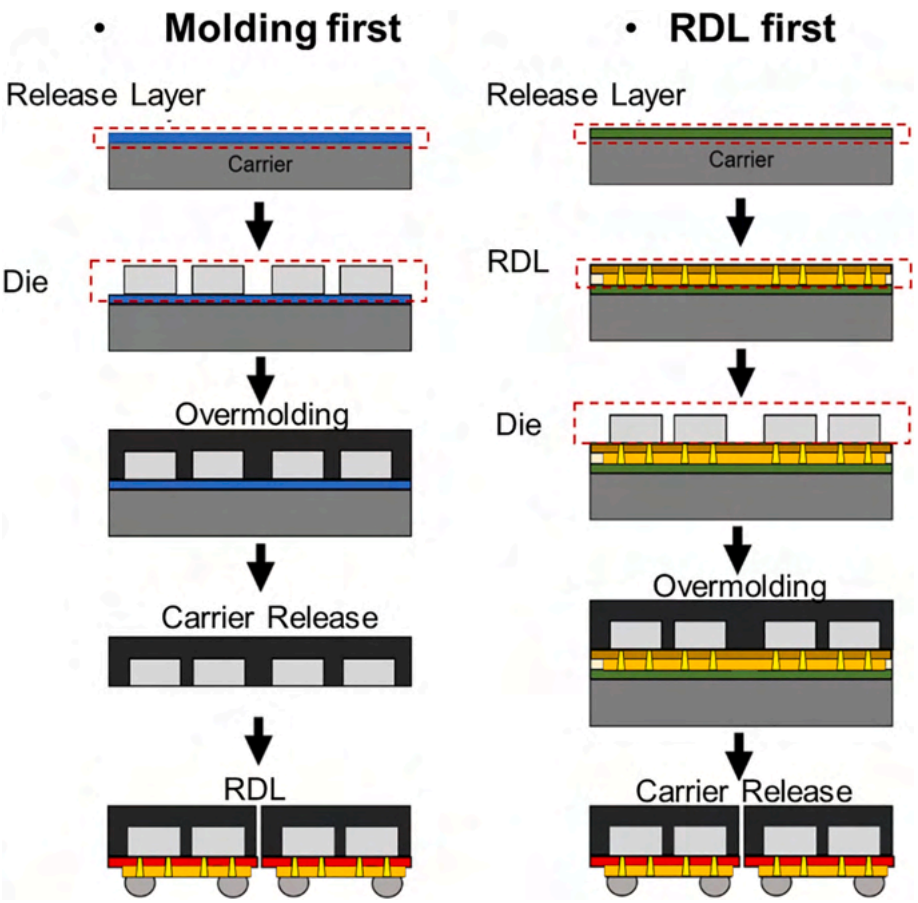

Fig. 1. Process flow chart of molding-first and RDL-first.

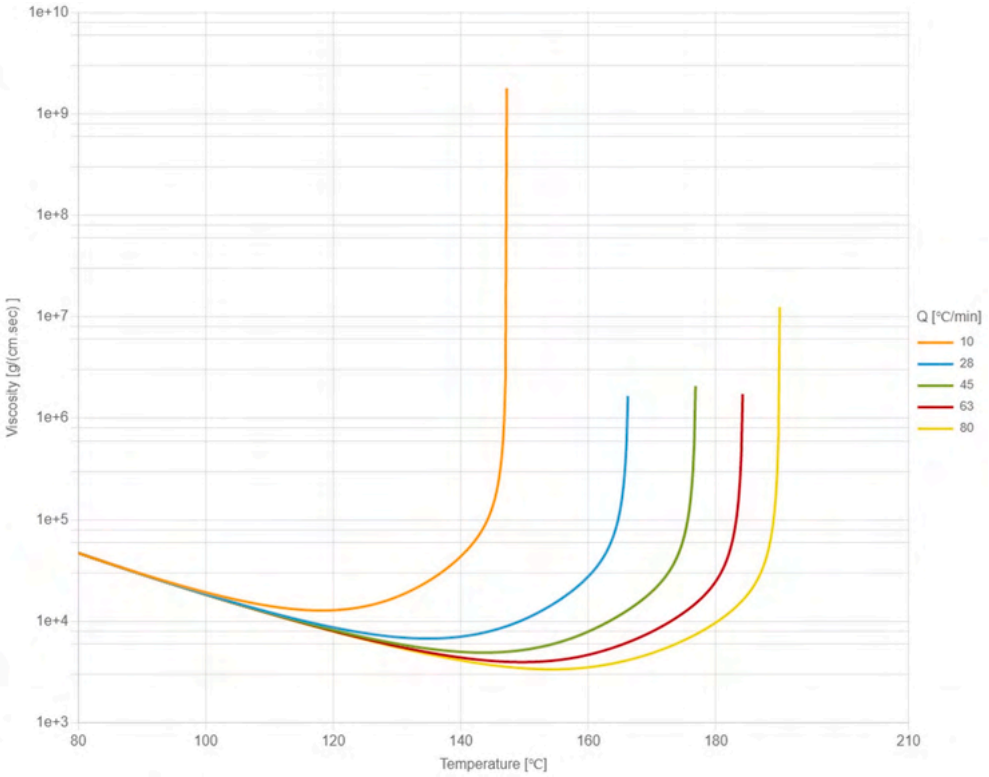

Fig. 2. Relationship between viscosity and temperature.

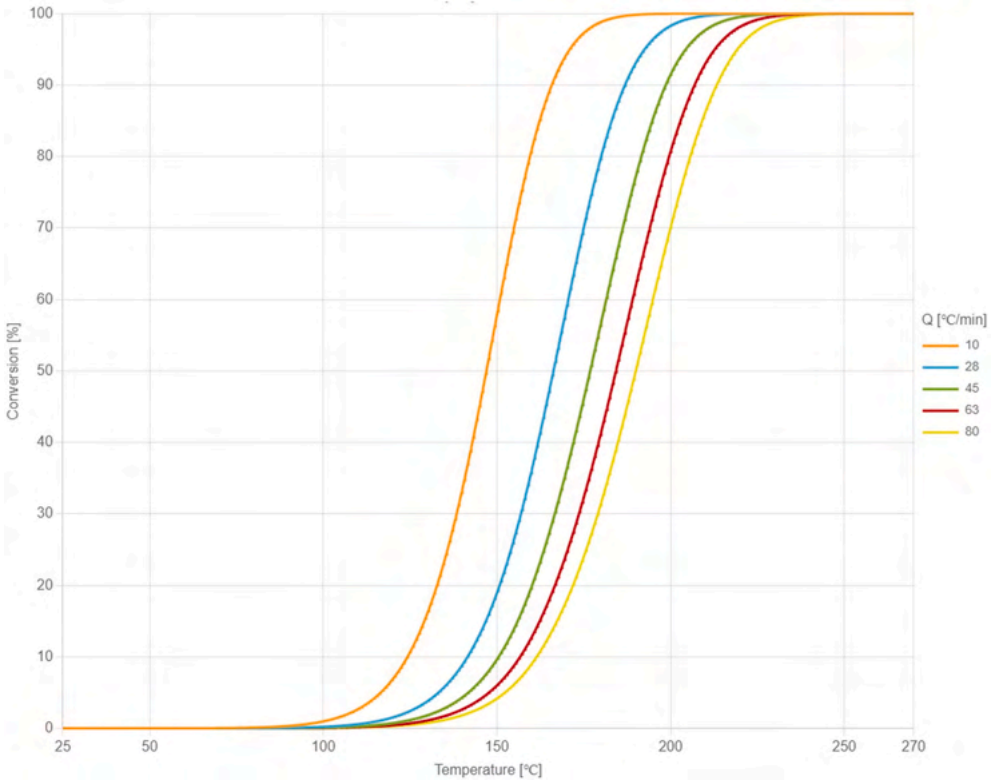

Fig. 3. Relationship between conversion and temperature.

significant factor. The *P–V–T–C* relationship was used to describe the behavior of EMC, as it effectively describes the intricate relationship between volume change, pressure, temperature, and the curing process [5].

In the past, Hwang developed a method that combines differential scanning calorimetry (DSC) and dynamic mechanical analysis (DMA) to accurately measure material properties [6]. By considering the maturity factor, Hwang derived the viscoelastic relationship known as the Dual

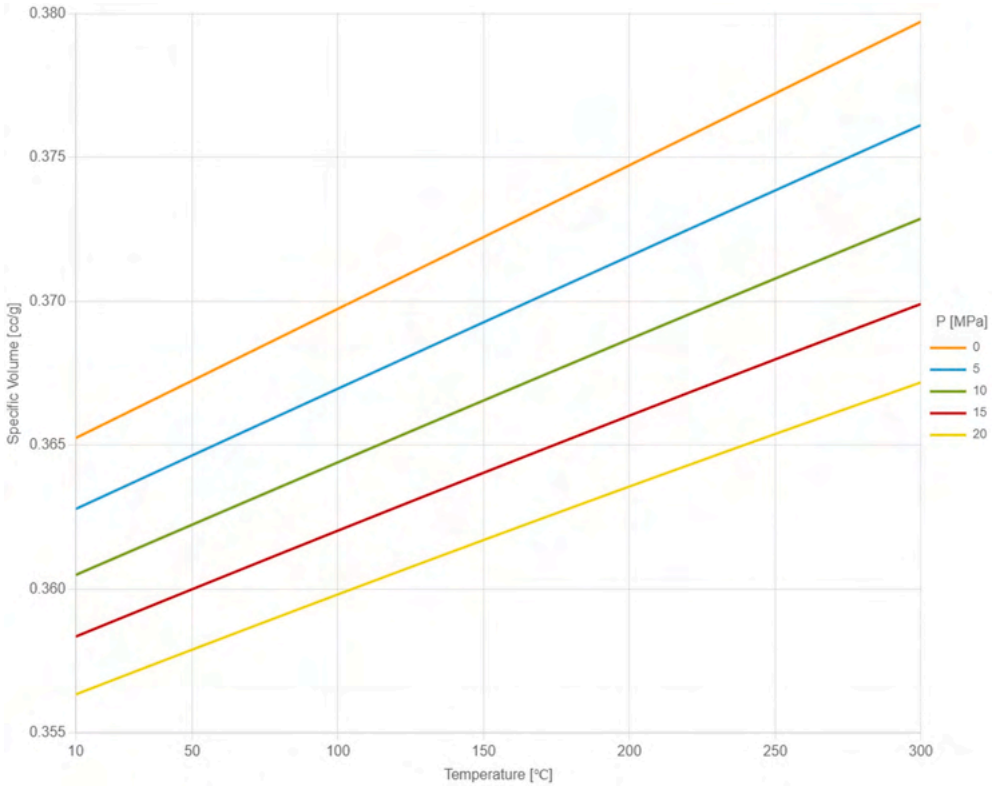

Fig. 4. *P–V–T–C* relationship.

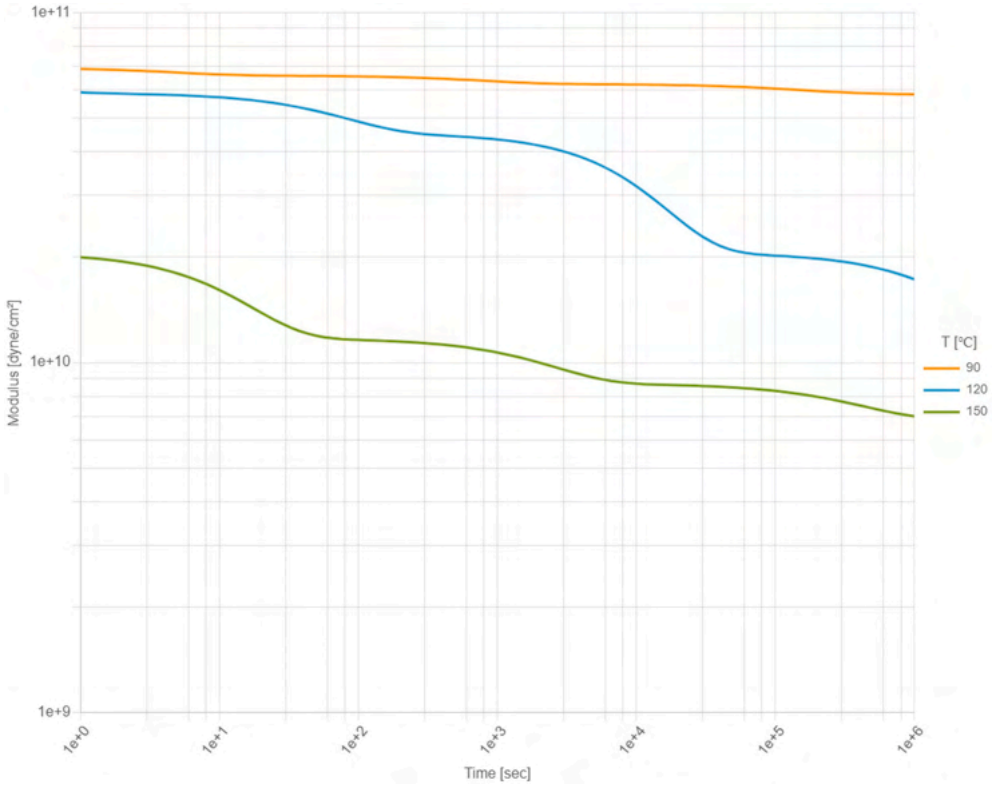

Fig. 5. Master curve of the relaxation modulus.

Table 1
Material properties used in the simulations.

Material	Young's modulus (GPa)		CTE (10^{-6}/°C)	Poisson's ratio	Density (g/cm^3)
Copper	132		18.7	0.4	9
Dielectric	3.72		48	0.36	2.16
Release layer	4.6		4.9	0.3	1.2
Glass	77		3.8	0.22	2.4
Die (Si)	131		2.8	0.26	2.33
EMC	22		11	0.33	0.68
Solder ball (Sn)	68	−40 °C	23	0.4	8
	57	25 °C			
	52	50 °C			
	39	125 °C			
PCB	27.5		16.5	0.42	2

Shift Factor model, which effectively describes the material properties. This model is particularly well-suited for describing the PMC process.

When conducting the thermal stress analysis of the RDL process, Lee [7] emphasized the importance of considering equivalent modeling to accurately calculate the reference temperature. Additionally, when analyzing the warpage of each layer in the RDL structure, it was observed that the RDL process exhibits significant warpage and residual stress issues that cannot be disregarded before molding [8]. Wu [9] mentioned that when analyzing package models with extremely thin thickness, the warpage error between the simulation and the experimental results tends to be more pronounced. This discrepancy is particularly notable during the process of removing the glass carrier.

In the fatigue model based on plastic strain, the Coffin–Manson empirical formula is most used to predict the reliability of IC components. Maier [10] enhanced the completeness of the Coffin–Manson formula by incorporating the cycle frequency, solder balls, and substrate temperature parameters. This modified version is referred to as the modified Coffin–Manson model. In IC components, the solder ball is typically the first location to experience fatigue failure. Therefore, the Anand model [11,12] is utilized to describe the viscoelastic properties of the solder ball.

In this paper, a reliability analysis procedure for FOPLP was established. This procedure incorporated the consideration of the residual stress induced during the fabrication processes. The reliability analysis procedure facilitates subsequent fatigue life calculations based on efficient exploration of the effects of process modeling and material modeling to find residual stress and warpage occurring during the manufacturing process.

2. Theory

2.1. Viscosity model

The cross Castro–Macosko model [13] was used for the viscosity calculation of EMC and considered both the temperature and the

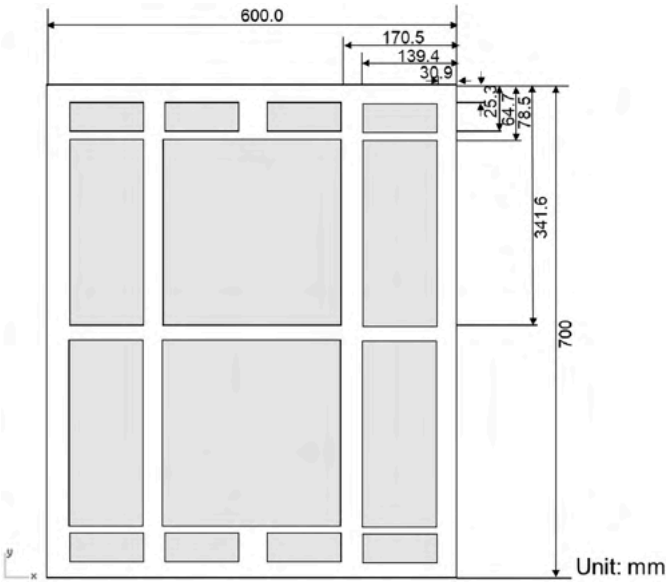

Fig. 7. Top view of geometry of the panel.

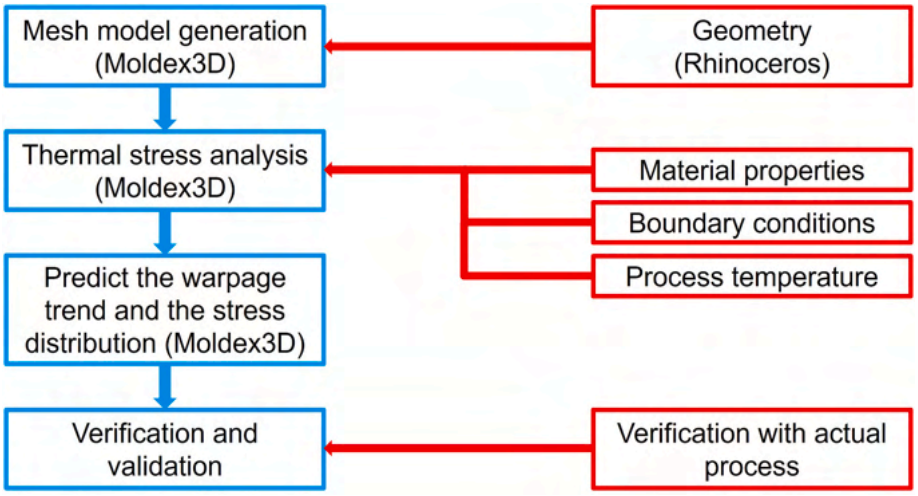

Fig. 6. Flow chart of RDL thermal stress analysis.

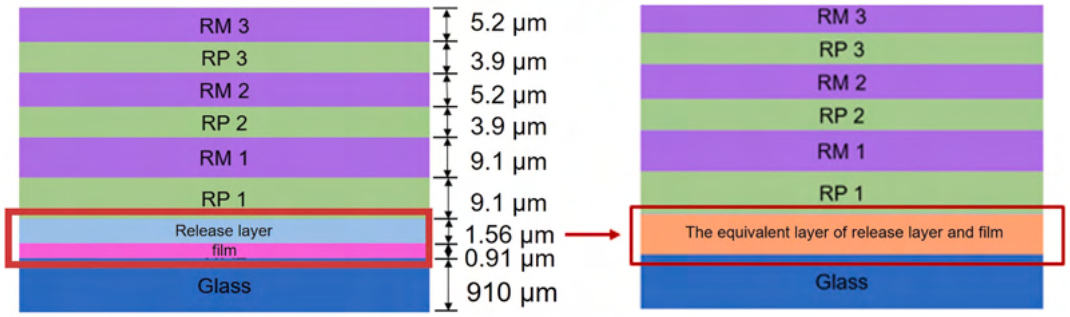

Fig. 8. Sectional diagram of the thermal stress analysis model of the panel and equivalent modeling for thin film layers.

Table 2
Copper content of RDL layers.

Layer	Copper content
RP 1	–
RM 1	30 %
RP 2	–
RM 2	15 %
RP 3	–
RM 3	8 %

conversion effects on viscosity in this study, as shown in Fig. 2:

$$\eta = \frac{\eta_0 \left(\frac{C_g}{C_g - C}\right)^{k_1 + k_2 C}}{1 + \left(\frac{\eta_0 \dot{\gamma}}{\tau^*}\right)^{1-n}} \tag{1}$$

$$\eta_0 = A \bullet exp\left(\frac{T_b}{T}\right) \tag{2}$$

C: degree of cure; η: viscosity; η_0: zero-shear-rate viscosity; $\dot{\gamma}$: shear strain rate; τ^*: critical shear stress; n: power law index; C_g: degree of cure at gel point; k_1, k_2, A, T_b: model constants.

2.2. Cure kinetics model

Kamal's model [14] was used for the cure kinetics calculation of EMC in this study; the model considered that the degree of curing was affected by both temperature and time, as shown in Fig. 3:

$$\dot{C} = \frac{dC}{dt} = (K_a + K_b \bullet C^m) \bullet (1 - C)^n \tag{3}$$

$$K_a = A \bullet exp\left(-\frac{T_1}{T}\right) \tag{4}$$

$$K_b = B \bullet exp\left(-\frac{T_2}{T}\right) \tag{5}$$

$\dot{C}$: cure reaction rate; C: degree of cure; A, B, m, n, K_a, K_b : model constants; E_a, E_b: activation energies; T_1, T_2: activation temperature.

2.3. P–V–T–C model

The P–V–T–C curve of EMC illustrates the specific volume variation of both mature and unripe states with respect to temperature at different pressures. The two-domain modified Tait model was used for establishing the P–V–T–C relation of EMC in this study, as shown in Fig. 4:

$$\frac{1}{V} = \frac{1}{V_{uncured}} \bullet (1 - C) + \frac{1}{V_{cured}} \bullet C \tag{6}$$

$$V_{uncured/cured} = V_0 \left[1 - \alpha \bullet ln\left(1 + \frac{P}{B}\right)\right] \tag{7}$$

$$V_0 = \begin{cases} b_{1S} + b_{2S}(T - b_5), \text{if } T \le T_{trans} \\ b_{1L} + b_{2L}(T - b_5), \text{if } T > T_{trans} \end{cases} \tag{8}$$

$$B = \begin{cases} b_{3S} \bullet exp[-b_{4S} \bullet (T - b_5)], \text{if } T \le T_{trans} \\ b_{3L} \bullet exp[-b_{4L} \bullet (T - b_5)], \text{if } T > T_{trans} \end{cases} \tag{9}$$

$$T_{trans}(P) = b_5 + b_6 \bullet P, \alpha = 0.0894 \tag{10}$$

C: degree of cure; V: specific volume; V_0: specific volume at zero-gauge pressure; B: accounts for pressure sensitivity of the material; b_6:

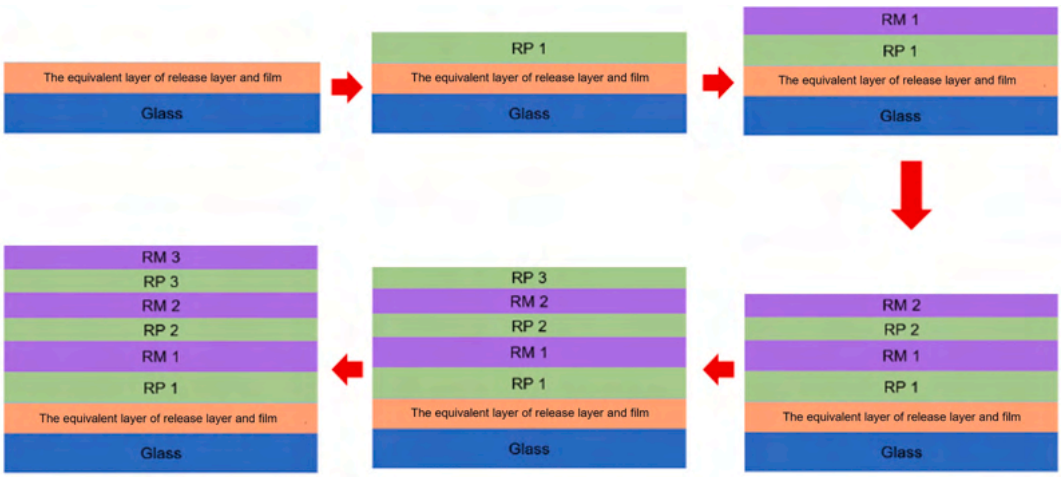

Fig. 9. Simulation process of RDL thermal stress analysis.

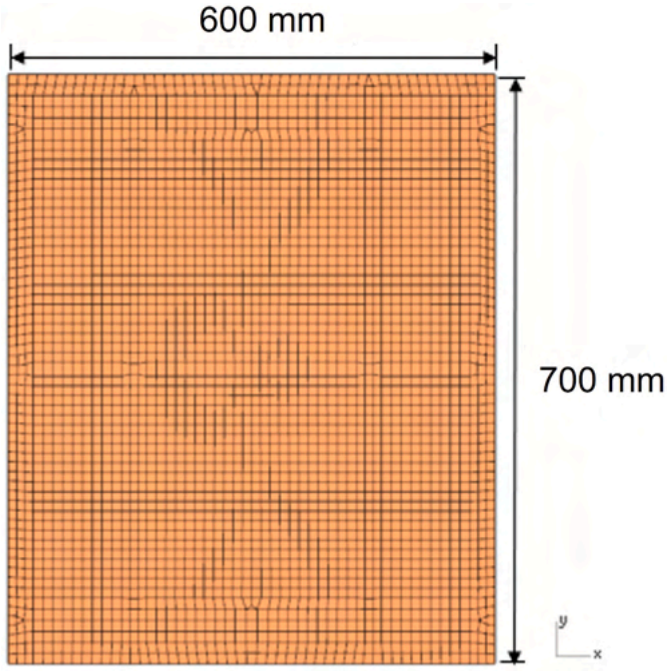

Fig. 10. Top view of mesh model used in simulation.

linear increase in T_{trans} with pressure; b_5: transition temperature at zero-gauge pressure.

2.4. Viscoelastic model

When a material exhibits characteristics of both a fluid and a solid, with properties encompassing both spring and damper behavior, it is commonly referred to as a viscoelastic material. The dual shift factor model was used for the viscoelastic calculation of EMC in this study [15], as shown in Fig. 5:

$$E(t) = E_\infty + \sum_{i=1}^{N} E_i \bullet exp\left(-\frac{t}{\lambda_i}\right) \tag{11}$$

$$\lambda_i(T) = \lambda_i(T_f) \bullet a_T(T) \bullet a_C(C) \tag{12}$$

$$a_T = \begin{cases} exp\left(\dfrac{-A_1(T-T_f)}{A_2+(T-T_f)}\right), \text{for } T \geq T^* \\ exp\left(\dfrac{\Delta H_T}{R}\left(\dfrac{1}{T}-\dfrac{1}{T_0}\right)\right), \text{for } T < T^* \end{cases} \tag{13}$$

Table 3
Number of mesh elements for six simulation processes.

Simulation	Structures	Number of elements
1.	Glass and the equivalent layer of the release layer and film	110,500
2.	Glass, the equivalent layer of the release layer and film, and RP 1	119,746
3.	Glass, the equivalent layer of the release layer and film, RP 1, and RM 1	132,026
4.	Glass, the equivalent layer of the release layer and film, RP 1–2, and RM 1–2	141,236
5.	Glass, the equivalent layer of the release layer and film, RP 1–3, and RM 1–2	150,446
6.	Glass, the equivalent layer of the release layer and film, RP 1–3, and RM 1–3	156,586

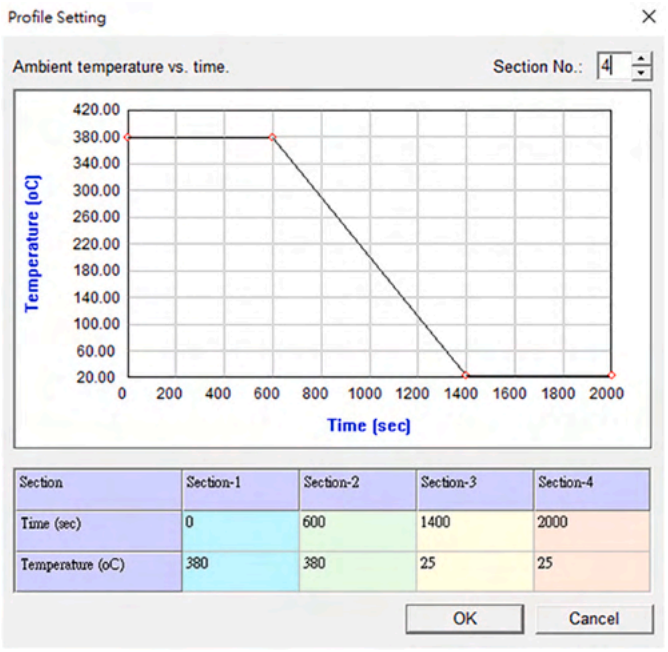

Fig. 11. Temperature setting of film.

$$a_C = exp\left(-\frac{\Delta H_C}{R}\left(\frac{1}{T_g(C)}-\frac{1}{T_{g1}}\right)\right) \tag{14}$$

$$T_g(C) = T_{g0} + \frac{\gamma C(T_{g1}-T_{g0})}{1-(1-\gamma)C} \tag{15}$$

$E(t)$: stress relaxation modulus; T_f: reference temperature; T^*: critical temperature; A_1, A_2: WLF model constants; $\Delta H_T/R$, $\Delta H_C/R$: active energy; T_g: glass transition temperature.

3. Simulations

This section presents a detailed overview of the various analyses

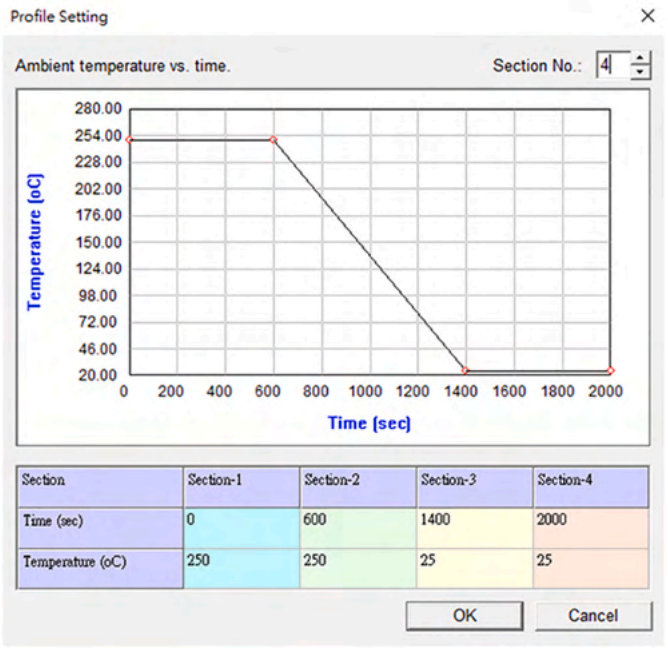

Fig. 12. Temperature setting of RDL.

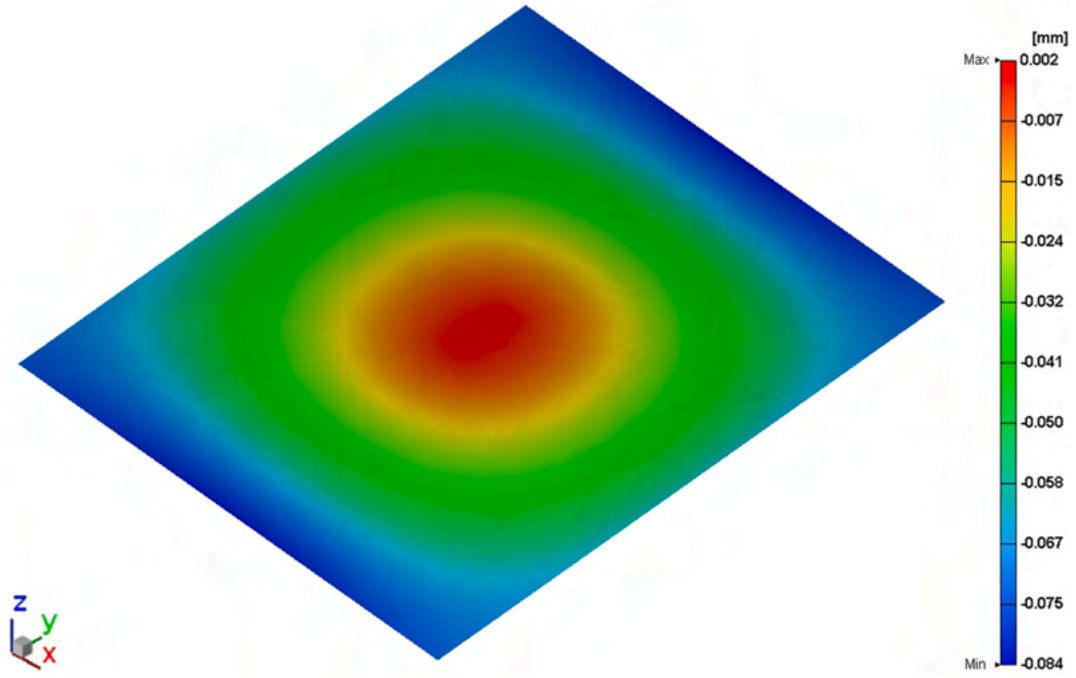

Fig. 13. Warpage analysis of stacked thin film layers on a glass carrier.

conducted in the study, including thermal stress analysis of the RDL process, compression molding analysis, PMC analysis, analysis of removing the glass carrier, and thermal cycle analysis. All the material properties used in the simulations of the research are listed in Table 1.

Assume all the materials used during RDL processes are isotropic, homogeneous, and linear elastic. There are two types of residual stress, one is macro residual stress, and the other is micro residual stress. Micro residual stress has small influence on stress states of an object and can be ignored during the simulation process.

EMC is assumed to be an isotropic, homogeneous, and linear elastic material during molding and to follow the relationship of Generalized Hook's Law. Furthermore, during PMC process, EMC isn't fully cure after molding and is assumed to be a viscoelastic material. Dual shift factor model was used to model the viscoelastic behavior of EMC in this study during PMC analysis.

3.1. *Thermal stress analysis of the RDL process*

This section presents an introduction of the geometry model, mesh model, and material properties of the RDL structure. The thermal stress

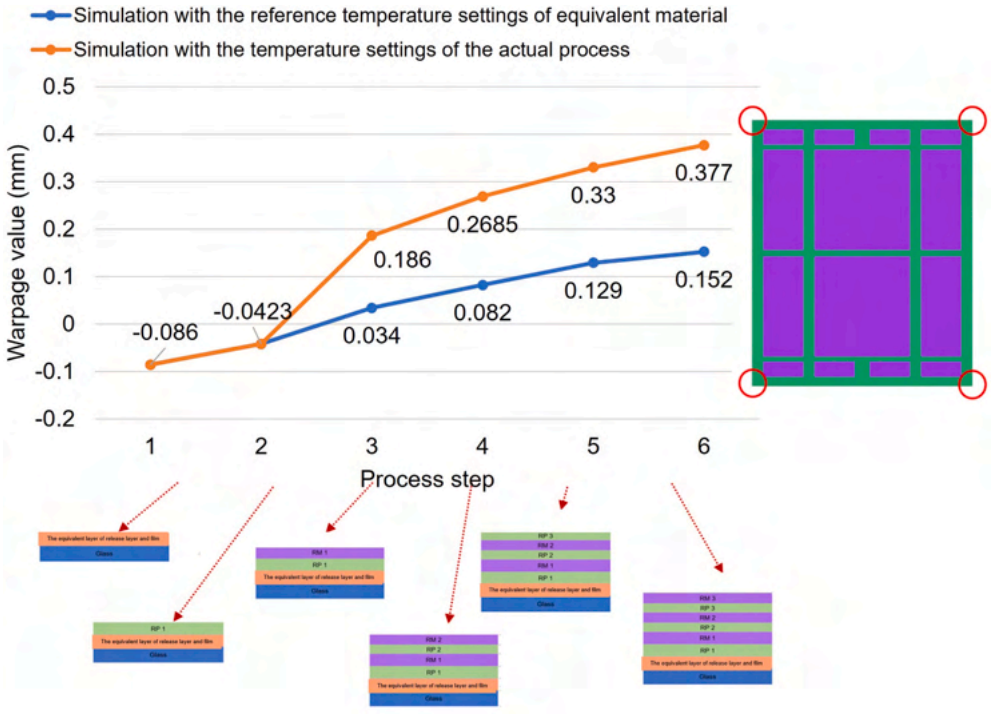

Fig. 14. Diagonal warpage results of six simulations.

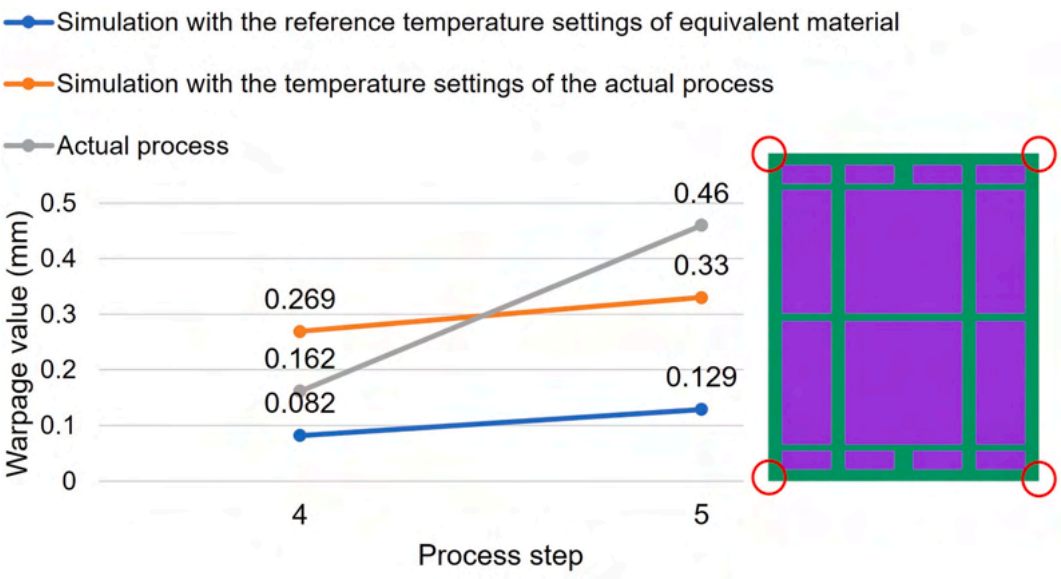

Fig. 15. Comparison of diagonal warpage results and actual process.

analysis of the RDL process was performed, starting from high-temperature conditions and gradually cooling down to room temperature. The analysis aimed to observe the residual stress, warpage trend, and warpage values of the RDL structure, and compare the results with the actual process. Fig. 6 shows a flow chart of the RDL thermal stress analysis.

3.1.1. Geometry model

The geometry model used for the thermal stress analysis of the RDL process and the equivalent material properties of the release layer and film, which were calculated by using the rule of mixtures, were applied in the simulation, as shown in Figs. 7 and 8. As shown in Fig. 7, the dark areas in the panel indicate that there're electrical circuits inside the RM layers and thus with copper content in those RM layers. The remaining white areas represent layers without copper content and with dielectric material only inside those RM layers. Table 2 presents the copper content of the RDL layers. As shown in Fig. 9, the RDL thermal stress analysis used six models in the analysis to simulate the warpage changes caused by structural stacking.

3.1.2. Mesh model and boundary condition

The top view of the mesh model is shown in Fig. 10. The mesh sizes were 12.2 mm in the simulations, and the number of mesh elements are shown in Table 3. Then, besides the effects of gravity, the boundary condition for simulations sets only one fixed displacement constraint at the center point of the model during thermal stress analysis of the RDL process.

3.1.3. Temperature settings

The temperature settings are shown in Figs. 11 and 12, which simulated the temperature settings of the actual process.

Lee [7] proposed an equivalent calculation of its process temperature and calculated the reference temperature of its equivalent material:

$$T_{eq_ref} = \frac{VE_{Cu}\alpha_{Cu}T_{ref_Cu} + (1-V)E_{PID}\alpha_{PID}T_{ref_PID}}{VE_{Cu}\alpha_{Cu} + (1-V)E_{PID}\alpha_{PID}} \quad (16)$$

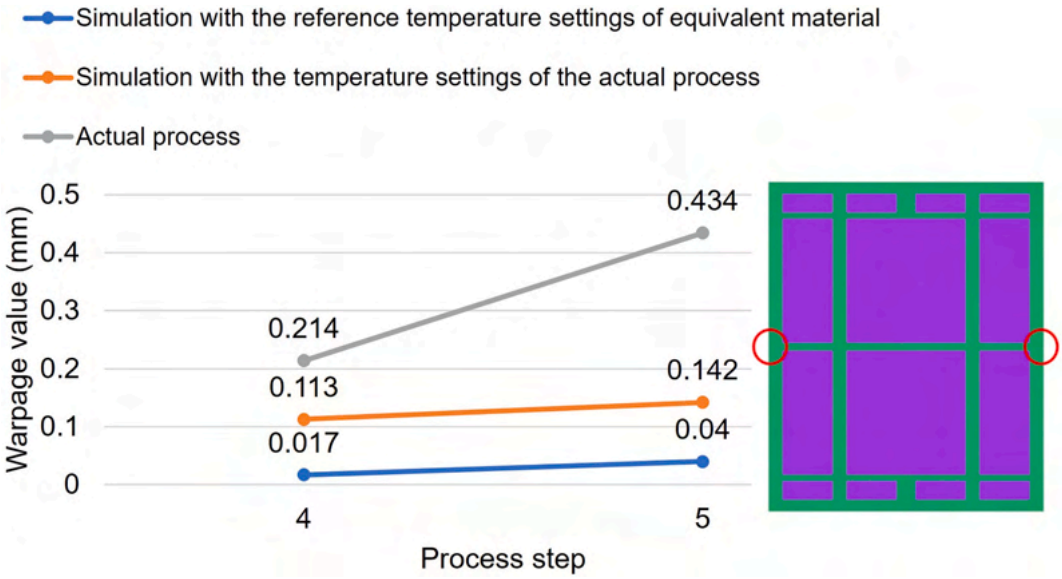

Fig. 16. Comparison of long-side warpage results and actual process.

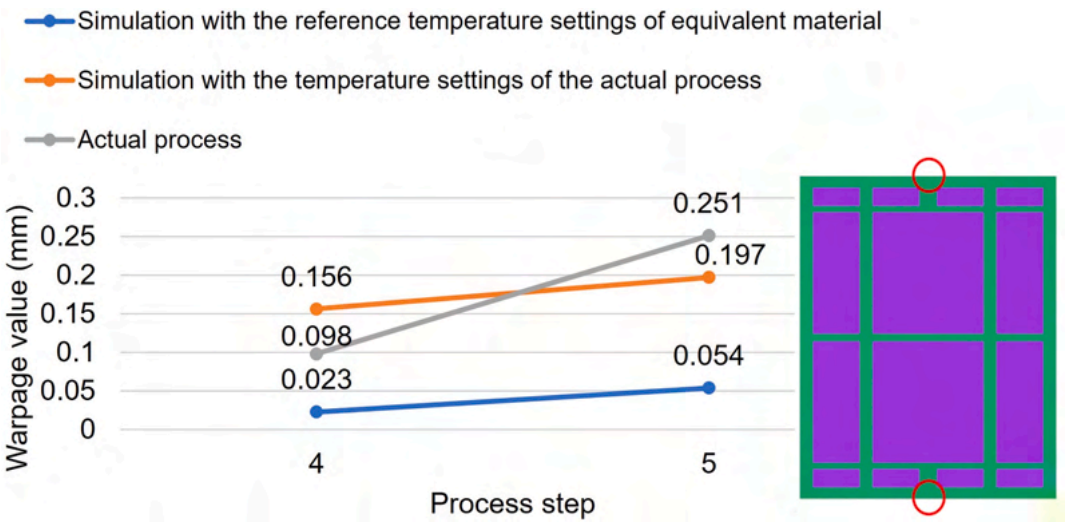

Fig. 17. Comparison of short-side warpage results and actual process.

where V denotes the copper content of RDL, α_{Cu} represents the CTE of copper, α_{PID} indicates the CTE of PID, E_{Cu} refers to the elastic modulus of copper, E_{PID} denotes the elastic modulus of PID, and T_{ref_Cu} and T_{ref_PID} represent the reference temperatures of copper and PID materials, respectively. The reference temperatures calculated using the above equation in the structural order were 380, 250, 113.23, 121, 130.02, and 132.1 °C.

3.1.4. Results

The warpage result of the analysis for the stacked thin film layers on a glass carrier, as shown in Fig. 13, was 86 μm and the warpage trend was concave down. The warpage results of six simulations are shown in Fig. 14. Figs. 15–17 present the simulation results for the comparison with the experimental values of the diagonal, long side, and short side, respectively.

In Fig. 14, the orange lines represent the simulation results with temperature settings of the actual RDL process and the blue lines indicate the simulation results with the reference temperature settings of equivalent material. As shown in step 2 of Fig. 14, warpage trends of both simulations show concave downward (cry) after depositing RP1 layer. Subsequently, when stacking RM1 layer to the structure as shown in step 3 of Fig. 14, the warpage trend changes from concave downward to concave upward (smile). Compared to the simulations with the reference temperature settings of equivalent material as shown in Fig. 14, warpage values with temperature settings of actual process show larger values due to the higher processing temperatures than the reference temperatures. Additionally, the gray line in Fig. 15 represents the actual measured warpage values from the experiments along the diagonal direction of the panel. Fig. 15 also shows that warpage values with actual process temperature settings in simulation would be better predicted than those with reference temperatures. Larger warpage value difference between the simulations and the actual process is found in long-side direction as shown in Figs. 15–17.

3.2. Compression molding and PMC analysis

The molding method used in this research was compression molding. This section discusses the simulation analysis of the compression molding and PMC process, as shown in Fig. 18.

3.2.1. Geometry model

Figs. 19, 20, and 21 show the geometry for the simulation analysis of compression molding in this study. The strip contained 85 packages, with each package containing two dies.

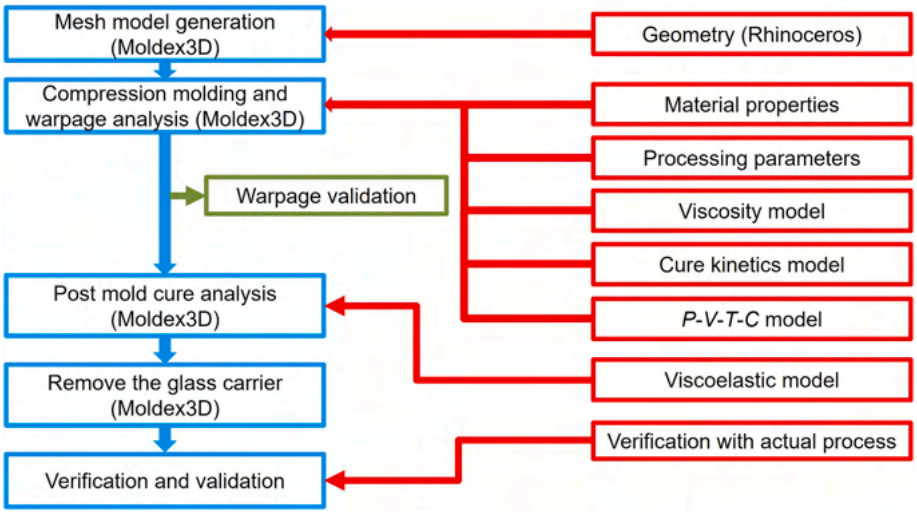

Fig. 18. Flow chart of IC packaging compression molding analysis.

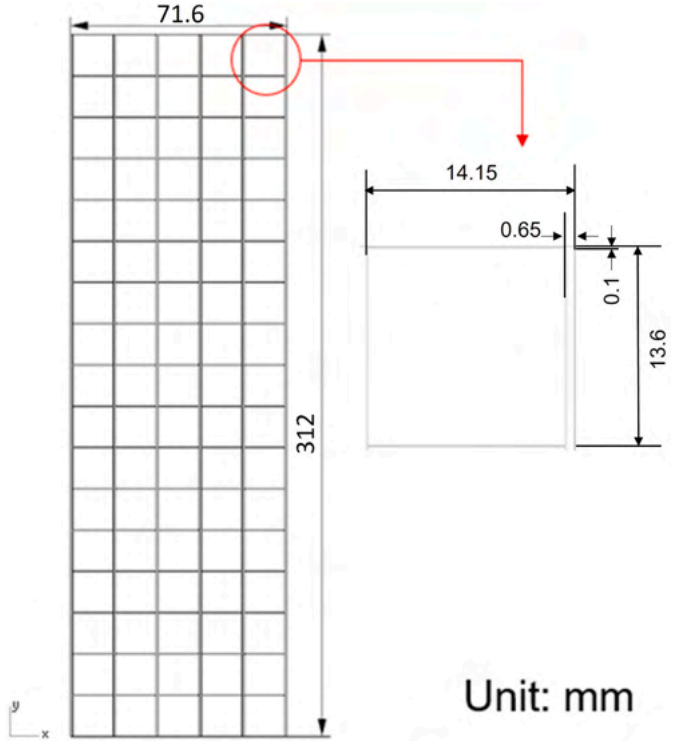

Fig. 19. Top view of the strip model.

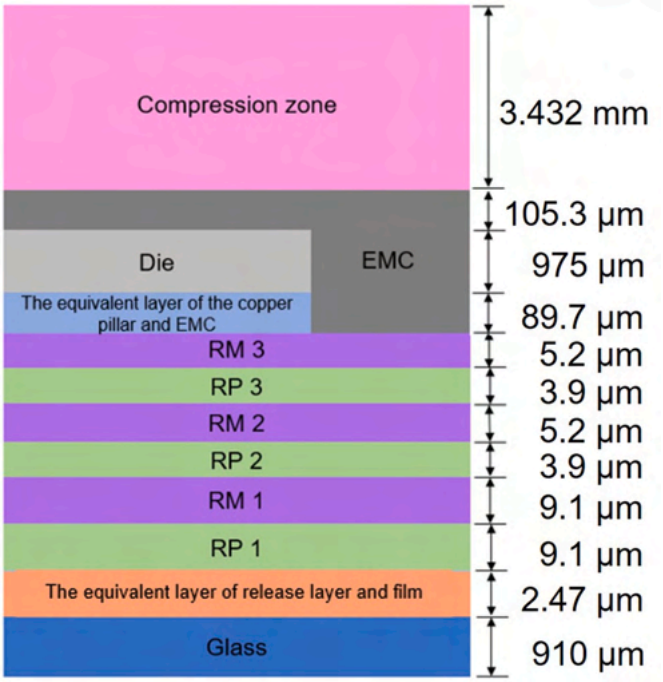

Fig. 21. Sectional diagram of the compression molding model.

3.2.2. Mesh model and boundary condition

The convergence analysis results are shown in Fig. 22, and the number of elements in the four models was 600,305; 2,051,145; 7,938,000; and 30,767,040, respectively. It was evident that as the number of meshes increased, the warpage value converged. Therefore, the following analysis used the model with a mesh size of 0.5 mm.

Fig. 23 shows the setting of boundary conditions during compression molding, moving the surface to fit the actual compression situation. In the PMC process, it is common practice to apply a heavy object on top of the product while maintaining it at a high temperature. This helps to reduce warpage. To better emulate the actual process, this study adopted a fixed bottom z displacement setting, as illustrated in Fig. 24.

3.2.3. Setting of process parameters

The process parameters of compression molding simulation and temperature settings are provided by Innolux Corporation. Both are set according to actual manufacturing parameters inside the factory, as shown in Table 4 and Fig. 25.

3.2.4. Molding and PMC warpage results

The warping deformation of EMC in this model was dominated by the *P–V–T–C* relationship. After molding as shown in Fig. 26, the maximum warpage deformation in the z direction was 9.16 mm, and the trend was concave upward. It's also found the degree of cure was approximately 82 %, which had not yet reached 100 %, so the PMC simulation analysis was carried out. After PMC analysis as shown in Fig. 26, the maximum warpage result was 7.945 mm, and the degree of cure had reached 100 %.

3.2.5. Consideration of the residual stress results of the RDL process

As shown in Fig. 27, the warpage trends in both figures considering and not considering residual stresses in RDL processes show concave

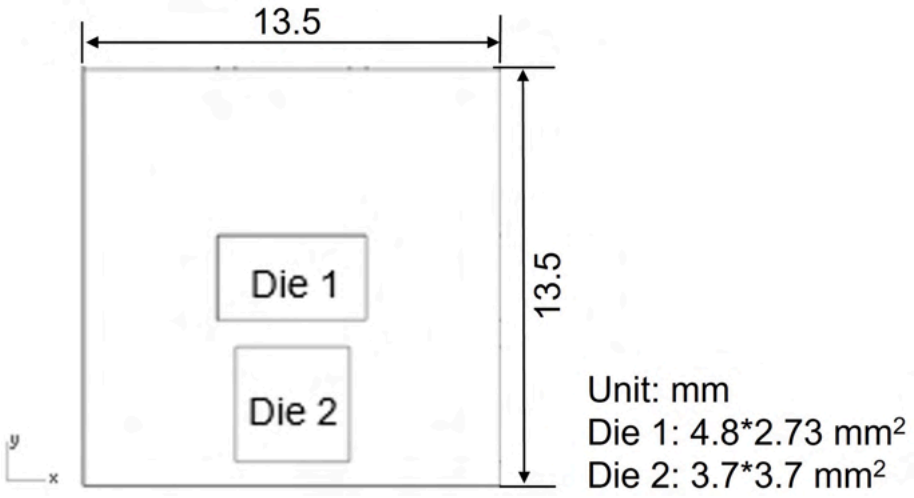

Fig. 20. Top view of the package.

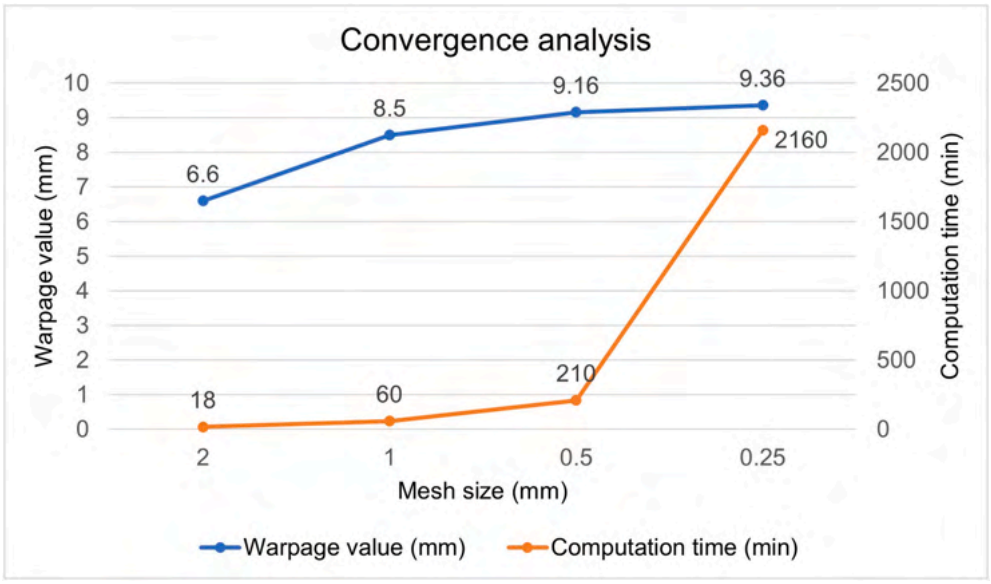

Fig. 22. Results of convergence analysis.

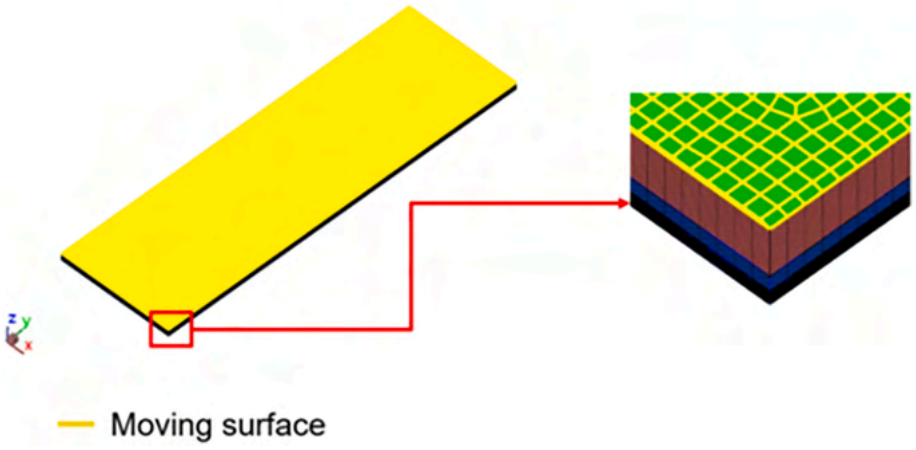

Fig. 23. Moving surface setting for compression molding.

upward. Additionally, the warpage values in both cases exhibited a difference of 3 μm only. Due to the nature of thin structure of the RDL layers, their impact on the overall structure is relatively small. Therefore, the residual stress due to the RDL process does not have a significant impact on the warpage value of the panel in this study.

3.3. Analysis results of removing the glass carrier

After the compression molding and PMC analysis, the next step was to remove the glass carrier. The warpage result obtained after removing glass carrier is shown in Fig. 28. The warpage value after removing the

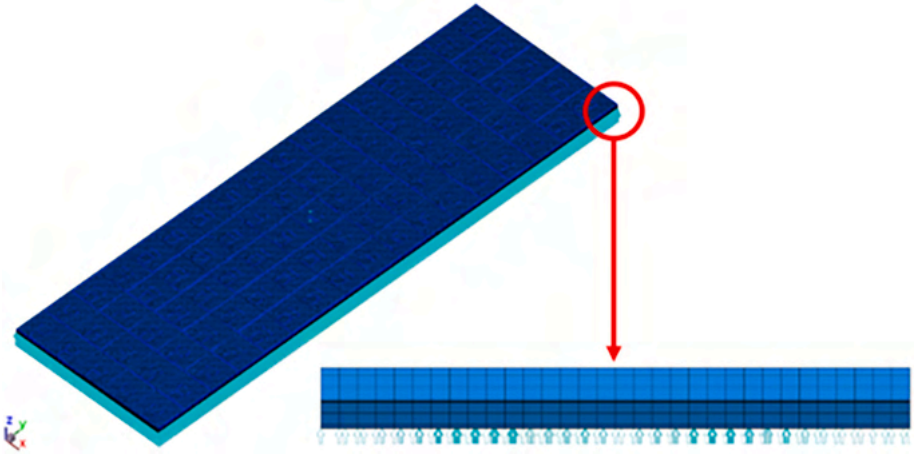

Fig. 24. PMC load when the temperature is maintained at a high value.

Table 4
Process parameters of compression molding simulation.

Process parameters	
Resin temperature	25 °C
Mold temperature	180 °C
Compression time	720 s
Compression force	24 tf
Initial conversion	0 %
Environment temperature	25 °C
Pre-heating time	0 s
Compression speed	0.132–0.036 mm/s

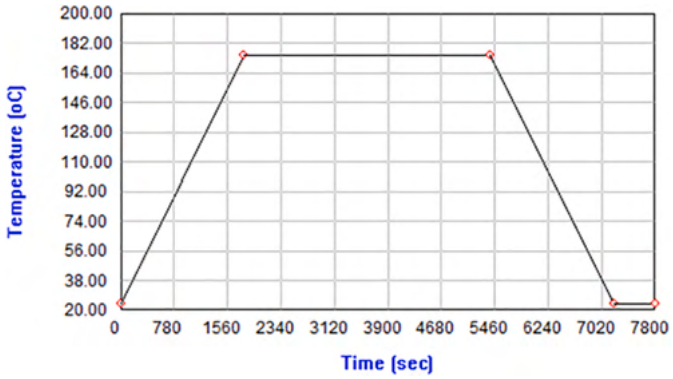

Fig. 25. Temperature setting of PMC simulation.

glass carrier changed from 7.945 mm to −2.173 mm, and the warpage trend changed from concave upward to concave downward.

4. Reliability analysis

4.1. Thermal cycle test (TCT)

In this study, Moldex3D was used to analyze TCT analysis, and the maximum residual stress of TCT analysis was brought into the plastic strain fatigue model to calculate the reliability of a single package.

4.1.1. Geometry model

The geometry model used for TCT analysis is shown in Figs. 29 and 30; this model was provided by InnoLux. The mesh model of TCT analysis is shown in Fig. 31.

4.1.2. Temperature cycle condition settings

As shown in Fig. 32, the first temperature curve is the temperature setting of the PMC process, and the second temperature curve is the reflow temperature setting of the solder ball. The analysis settings of these two processes were returned to 25 °C after the high-temperature treatment. The temperature curve from 10,200 s to 18,900 s was the temperature setting of the thermal cycle. In the thermal cycle setting, all the heating and cooling times were 900 s. The dwell time was 900 s.

4.1.3. Results

Upon the completion of TCT analysis, it could be inferred from Fig. 33 that the maximum Von Mises stress value was 147.309 MPa and was found to be located in the solder balls. The maximum stress value was observed at 13800 s. The stress values at each stage of TCT analysis are shown in Fig. 34. The blue line represents the temperature curve, and the orange bars indicate the stress values under different temperatures. It can be observed that as time progresses, the temperature first drops from 25 °C to −40 °C, but the stress value didn't change a lot due to the structure of the package. Next, the stress values increase with the temperature rises from −40 °C to 125 °C due to thermal expansion.

4.2 Reliability

The fatigue life of a product is usually calculated to analyze the structure that is the most prone to damage in the product, so this research focused on the calculation of the reliability of the structure of the solder ball. The results of TCT analysis were used as the initial conditions of the reliability analysis, and the maximum stress results were substituted into the Ramberg–Osgood model to calculate the plastic strain of the solder ball [16,17]:

$$\Delta\varepsilon_p = \frac{\sigma}{E} + \left(\frac{\sigma}{\sigma_0}\right)^n \tag{17}$$

where $\Delta\varepsilon_p$ denotes the plastic equivalent strain, E represents Young's modulus, σ_0 indicates the yield stress, and n refers to the material constants, $n = 5.4$.

Upon the substitution of the maximum von Mises stress value, which was 147.309 MPa, into the equation above, the calculated plastic strain

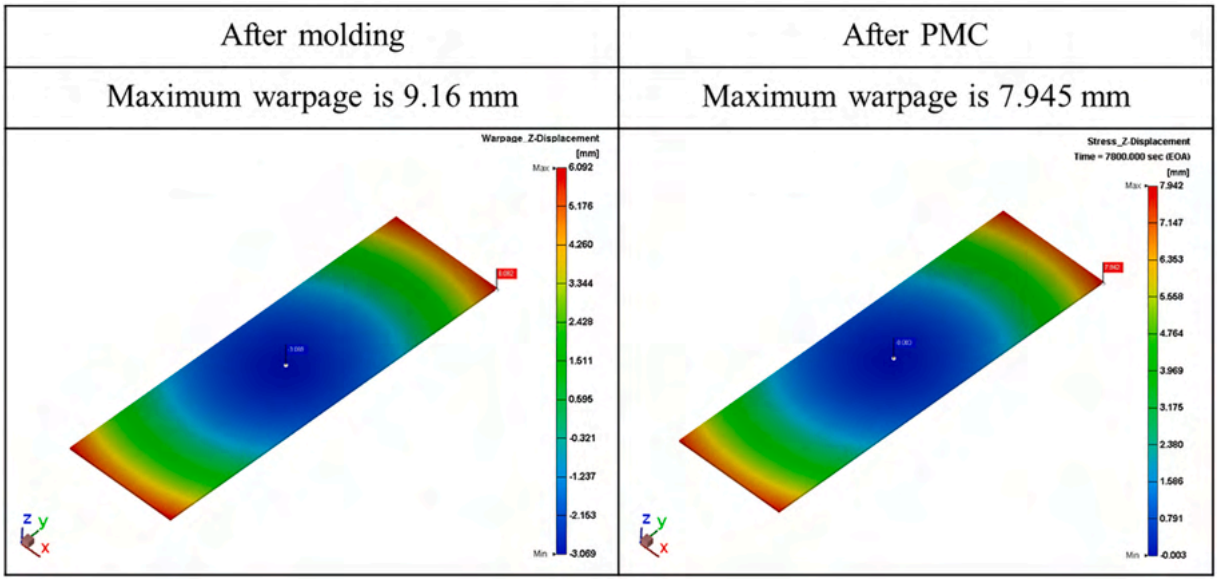

Fig. 26. Warpage results after molding and PMC simulations.

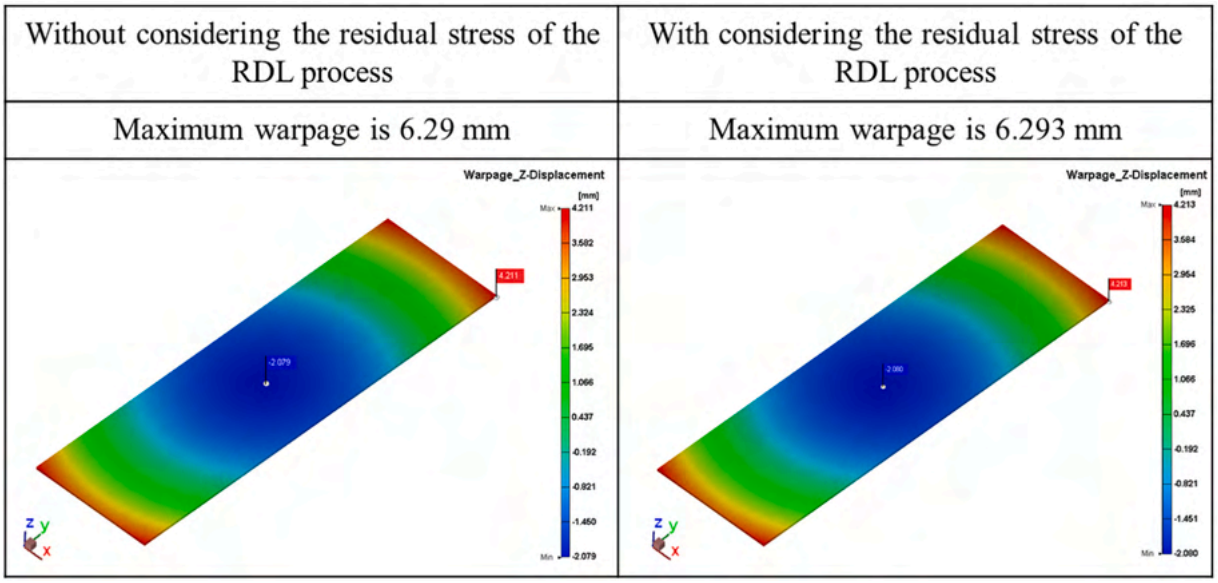

Fig. 27. Warpage results with and without considering the residual stress of the RDL process.

was determined to be 0.026. Substituting the above calculated results into the modified Coffin–Manson model enabled the calculation of the fatigue life value, where T_m was 42.5 °C, t_D was 900 s, and $\dot{\varepsilon_f}$ was 0.279 [18]:

$$C_f = -0.442 - 6 \times 10^{-4} \times 42.5 + 1.74 \times 10^{-2} ln\left(1 + \frac{360}{900}\right) = -0.4616 \tag{18}$$

$$N_f = \frac{1}{2}\left(\Delta\varepsilon_p \Big/ 2\dot{\varepsilon_f}\right)^{1/C_f} = 417 \tag{19}$$

where $\Delta\gamma$ denotes the inelastic strain range, T_m represents the average cyclic temperature, and t_D indicates the cycle dwell time.

The fatigue life obtained using the modified Coffin–Manson model was 417 cycles, which had an error 16.6 % compared with that of the approximately 500 cycles in the actual process.

5. Conclusions

In this study, a warpage and stress simulation procedure and a reliability analysis process considering residual stresses due to fabrication process for FOPLP were proposed and established. RDL fabrication, compression molding, PMC and glass removal processes were considered in this paper for warpage and stress calculations. Then, TCT reliability analysis considering the residual stresses of all the processes was carrying out to predict the lifespan of the package.

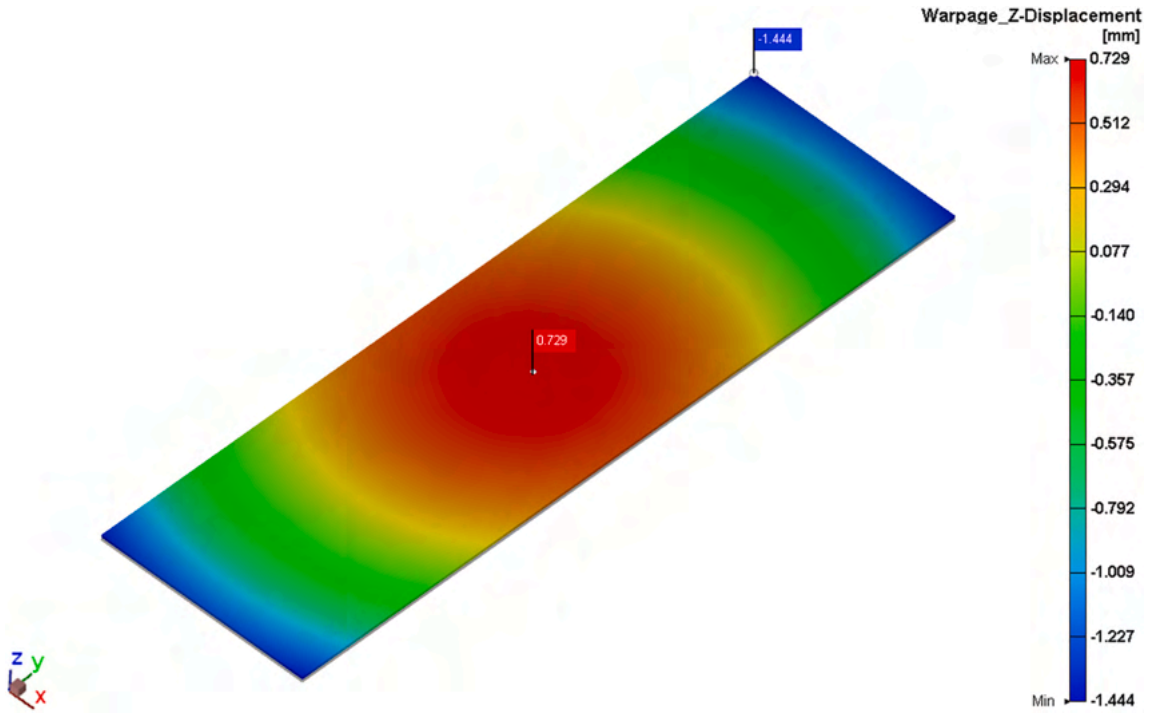

Fig. 28. Warpage results after removing the glass carrier.

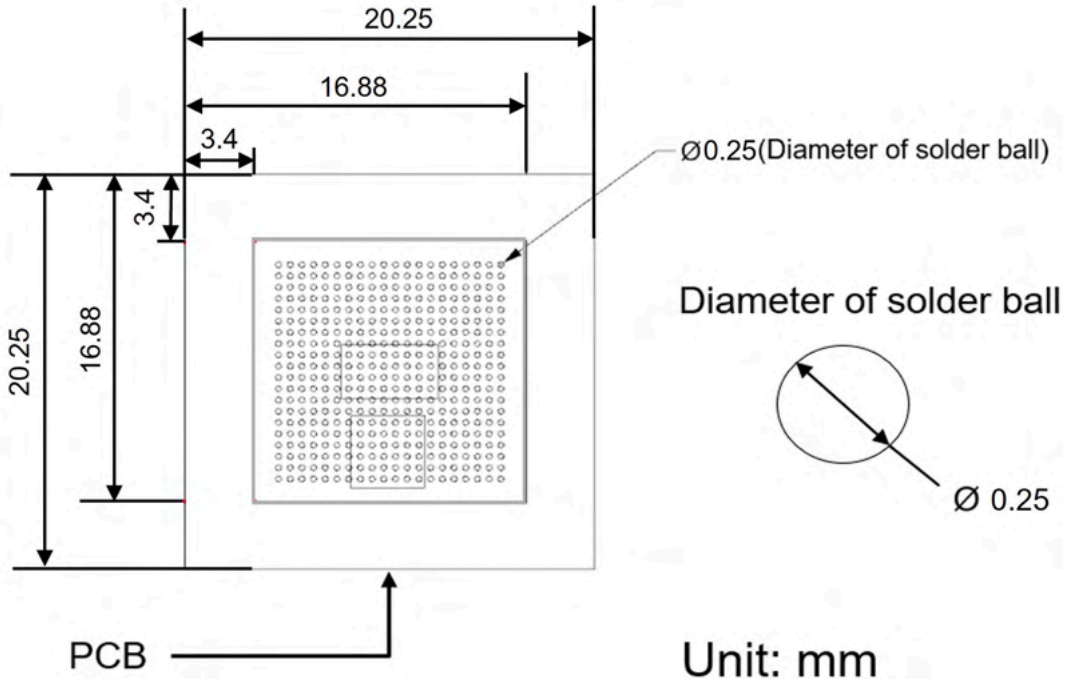

Fig. 29. Top view of TCT analysis model.

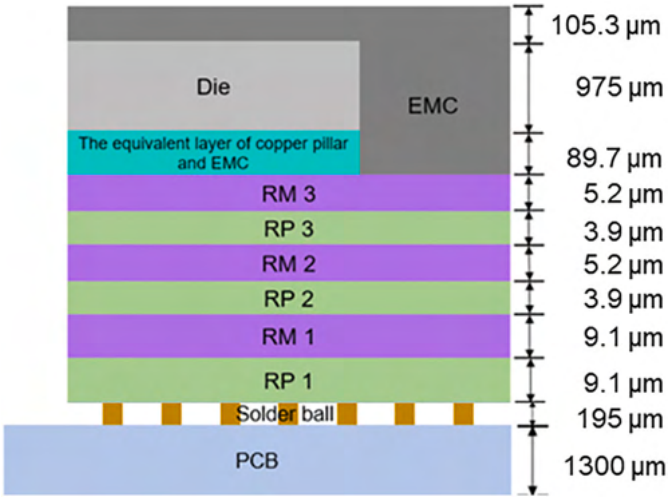

Fig. 30. Sectional diagram of TCT analysis model.

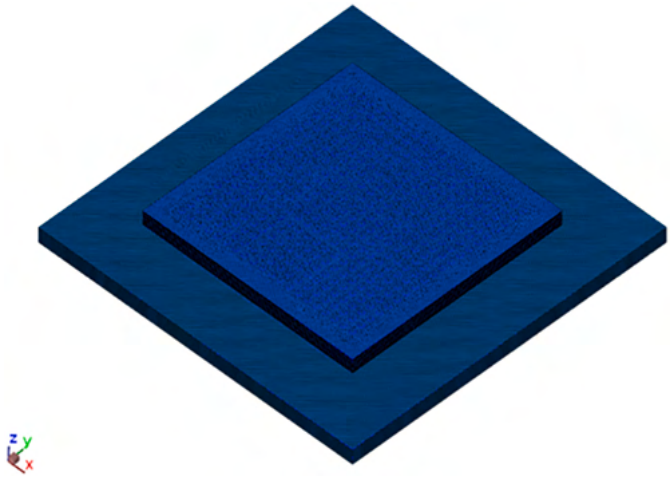

Fig. 31. Mesh model for TCT analysis.

In the RDL thermal stress analysis, warpage values with temperature settings of actual process show larger values compared to the simulation with the reference temperature settings of equivalent material. But both cases show similar warpage trend.

According to the warpage results of compression molding, the maximum warpage value was 9.16 mm, and the warpage trend was concave upward. In the PMC analysis, the maximum warpage value changed from 9.16 mm after compression molding to 7.945 mm after PMC. The residual stress results in RDL process were brought into the subsequent compression molding simulation as the initial condition and it was found that the residual stress from RDL process did not have a significant impact on the warpage values during the compression molding process. The warpage values considering and not considering RDL induced residual stress exhibited a difference of only 3 μm. After removing the glass carrier, the warpage result was −2.173 mm, and the warpage trend changed from concave upward to concave downward.

For TCT analysis, thermal stress analysis considering residual stress

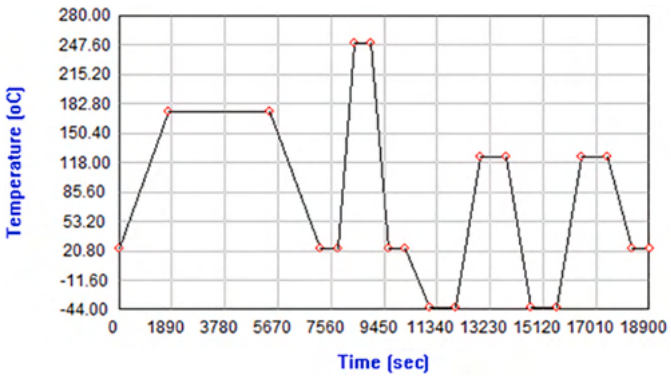

Fig. 32. Temperature cycle curve.

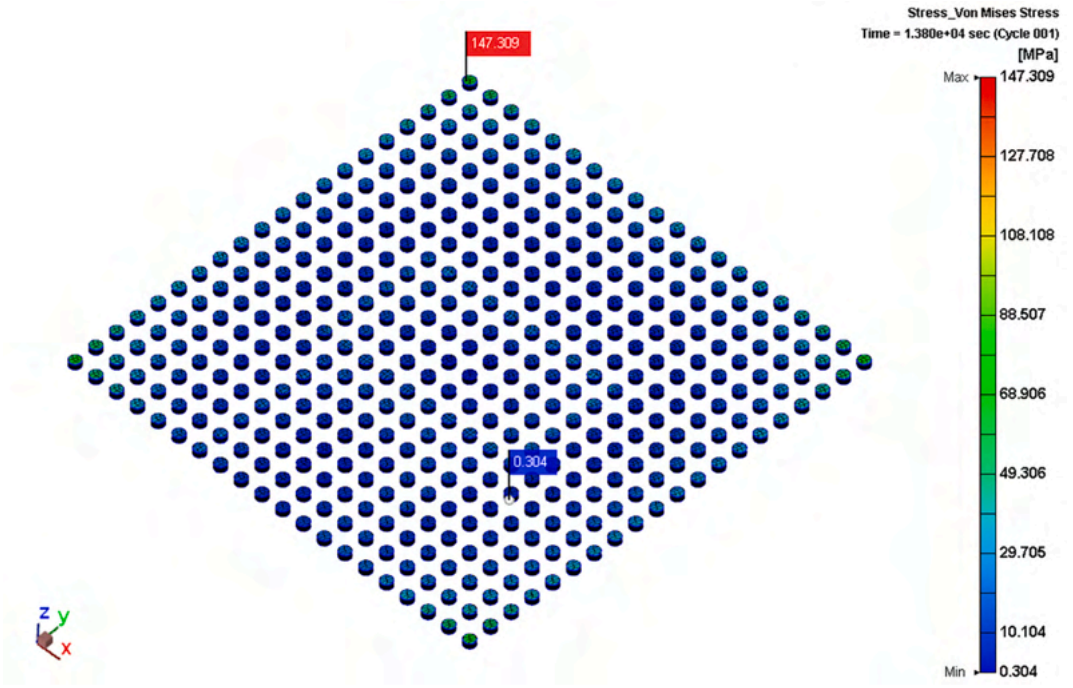

Fig. 33. Maximum stress value of TCT analysis.

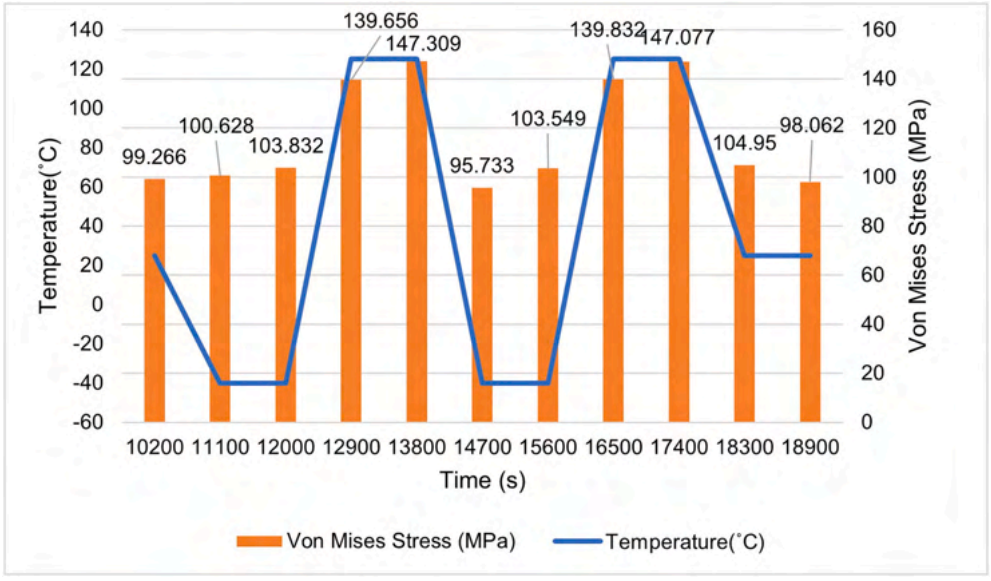

Fig. 34. Stress values at each stage of TCT analysis

after PMC was carried to calculate the maximum von Mises stress. It was found that solder balls were the most likely spots to fail. In this study, the maximum stress result for the solder ball structure was 147.309 MPa. Finally, the modified Coffin–Manson model was used to calculate the fatigue life. The fatigue life of the final product in this research was 417 cycles, which had an error 16.6 % compared with the fatigue life of approximately 500 cycles in the actual process. This reliability analysis procedure facilitates subsequent fatigue life calculations based on efficient exploration of the effects of process modeling and material modeling to find residual stress and warpage occurring during the manufacturing process.

CRediT authorship contribution statement

Chia-Wei Liang: Formal analysis, Methodology, Writing – original draft, Writing – review & editing. **Yu-Chi Sung:** Formal analysis, Methodology, Writing – review & editing. **Sheng-Jye Hwang:** Methodology, Supervision, Writing – original draft, Writing – review & editing. **Ming-Hsiang Shih:** Methodology, Supervision, Validation. **Wen-Hsiang Liao:** Methodology, Supervision, Validation. **Te-Hsun Lin:** Methodology, Validation. **Dong-Yan Yang:** Methodology, Validation.

Declaration of competing interest

The authors declare the following financial interests/personal relationships which may be considered as potential competing interests:

Sheng-Jye Hwang reports financial support was provided by Testing Center, Innolux Corporation, Tainan, Taiwan. If there are other authors, they declare that they have no known competing financial interests or personal relationships that could have appeared to influence the work reported in this paper.

References

[1] Motohashi Norikazu, Kimura Takehiro, Mineo Kazuyuki, Yamada Yusuke, Nishiyama Tomohiro, Shibuya Koujiro, et al. System in wafer-level package technology with RDL-first process. In: 2011 IEEE 61st Electronic Components and Technology Conference; 2011. p. 59–64. https://doi.org/10.1109/ECTC.2011.5898492.

[2] Lau John H, Ko Cheng-Ta, Yang Kai-Ming, Peng Chia-Yu, Xia Tim, Lin Puru Bruce, et al. Panel-level fan-out RDL-first packaging for heterogeneous integration. IEEE Trans Compon Packag Manuf Technol 2020;v10(7):1125–37. https://doi.org/10.1109/TCPMT.2020.2996658.

[3] Braun T, Raatz S, Voges S, Kahle R, Bader V, Bauer J, et al. Large area compression molding for fan-out panel level packing. In: 2015 IEEE 65th Electronic Components and Technology Conference; 2015. p. 1077–83. https://doi.org/10.1109/ECTC.2015.7159728.

[4] Hong L-C, Hwang S-J. Study of warpage due to PVTC relation of EMC in IC packaging. IEEE Transactions on Components and Packaging Technologies 2004; v27(2):291–5. https://doi.org/10.1109/TCAPT.2004.828579.

[5] Chang Y-S, Hwang S-J, Lee H-H, Huang D-Y. Study of PVTC relation of EMC. J Electron Package 2002;v124(4):371–3. https://doi.org/10.1115/1.1498266.

[6] Lee C-C, Wang C-W, Chen C-Y. Comparison of mechanical modeling to warpage estimation of RDL-first fan-out panel-level packaging. IEEE Trans Compon Packag Manuf Technol 2022;v12(7):1100–8. https://doi.org/10.1109/TCPMT.2022.3175953.

[7] Lee Chang-Chun, Wang Chi-Wei, Lee Chia-Chi, Chen Chin-Yi, Chen Yu-Hua, Lee Hung-Chih, et al. Warpage estimation of heterogeneous panel-level fan-out package with fine line RDL and extreme thin laminated substrate considering molding characteristics. In: 2021 IEEE 71st Electronic Components and Technology Conference; 2021. p. 1500–4. https://doi.org/10.1109/ECTC32696.2021.00238.

[8] Wu M-L, Lan J-S. Simulation and experimental study of the warpage of fan-out wafer-level packaging: the effect of the manufacturing process and optimal design. IEEE Trans Compon Packag Manuf Technol 2018;v9(7):1396–405. https://doi.org/10.1109/TCPMT.2018.2889930.

[9] Motohashi Norikazu, Kimura Takehiro, Mineo Kazuyuki, Yamada Yusuke, Nishiyama Tomohiro, Shibuya Koujiro, et al. System in wafer-level package technology with RDL-first process. In: 2011 IEEE 61st Electronic Components and Technology Conference; 2011. p. 59–64. https://doi.org/10.1109/ECTC.2011.5898492.

[10] Chauhan P, Osterman M, Lee SR, Pecht M. Critical review of the Engelmaier model for solder joint creep fatigue reliability. IEEE Transactions on Components and Packaging Technologies 2009;v32(3):693–700. https://doi.org/10.1109/TCAPT.2009.2030983.

[11] Anand L. Constitutive equations for the rate-dependent deformation of metals at elevated temperatures. J Eng Mater Technol 1982;v104(1):12–7. https://doi.org/10.1115/1.3225028.

[12] Brown SB, Kim KH, Anand L. An internal variable constitutive model for hot working of metals. Int J Plasticity 1989;v5(2):95–130. https://doi.org/10.1016/0749-6419(89)90025-9.

[13] Castro JM, Macosko CW. Kinetics and rheology of typical polyurethane reaction injection molding systems. SPE Tech Paper 1980;v26:434–8.

[14] Kamal MR, Ryan ME. In: Isayev AI, editor. Injection and Compression Molding Fundamentals. New York: Marcel Dekker; 2017. Chapter 4.

[15] Lin Y-J, Hwang S-J, Lee H-H, Huang D-Y. Modeling of viscoelastic behavior of an epoxy molding compound during and after curing. IEEE Trans Compon Packag Manuf Technol 2011;v1(11):1755–60. https://doi.org/10.1109/TCPMT.2011.2165339.

[16] Jenq S-T, Chang H-H, Lai Y-S, Tsai T-Y. High strain rate compression behavior for Sn–37Pb eutectic alloy, lead-free Sn–1Ag–0.5 Cu and Sn–3Ag–0.5 Cu alloys. Microelectronics Reliability 2009;v49(3):310–7. https://doi.org/10.1016/j.microrel.2009.01.002.

[17] Nguyen TT, Park S. Characterization of elasto-plastic behavior of actual SAC solder joints for drop test modeling. Microelectronics Reliability 2011;v51(8):1385–92. https://doi.org/10.1016/j.microrel.2011.03.019.

[18] Salmela O, Andersson K, Perttula A, Särkkä J, Tammenmaa M. Re-calibration of Engelmaier's model for leadless, lead-free solder attachments. Quality and Reliability Engineering International 2007;v23(4):415–29. https://doi.org/10.1002/qre.810.